International Journal of Heat and Mass Transfer 52 (2009) 5285–5292

Contents lists available at ScienceDirect

International Journal of Heat and Mass Transfer

journal homepage: www.elsevier.com/locate/ijhmt

Effect of pulsed magnetic field on superalloy melt

Xiaoping Ma, Yuansheng Yang *, Bin Wang

Institute of Metal Research, Chinese Academy of Sciences, Shenyang 110016, China

ARTICLE INFO

Article history:
Received 24 December 2008
Received in revised form 1 June 2009
Accepted 24 June 2009
Available online 27 August 2009

Keywords:
Pulsed magnetic field
Transient finite element analysis
Magnetic force distribution
Flow field
Joule heat distribution

ABSTRACT

In order to investigate the magnetic force distribution, flow field distribution and Joule heat distribution under the pulsed magnetic field (PMF), transient numerical simulation was carried out. Results show that the magnetic pressure force appears in the inner of the melt, while the magnetic pull force and the magnetic pressure force appear alternately in the exterior of the melt, which is caused by the skin vortex current. The axial direction magnetic force results in the convection of the melt. The radial direction magnetic force produces vibration of the melt. The vibration will diffuse and superpose to produce the pressure wave. Finally, the fluctuation of the melt is caused by the pressure wave. The Joule heat produced by pulsed magnetic field concentrates near the surface of the melt in the pulse applying period.

1. Introduction

The microstructure can be refined by the electromagnetic field applied in the solidification process, which will improve the properties of casting. It is notable that electromagnetic vibration can significantly refine solidified microstructure [1–6]. Recently, pulsed magnetic field (PMF) was applied to microstructure refinement and showed significant refinement effect [7–9]. The PMF is favorable because it is simple in equipment and easy to control. However, the variation of magnetic force and the flow field distribution with the magnetic pulse in the whole period is not clear because the PMF is transient, variable and complex. Because of experimental restriction, it is hard to solve those questions through experiment observation. But numerical simulation provides an effective analysis for experiment and industry production. The numerical analysis can contribute to understanding the mechanism why the PMF can refine microstructure. Kolesnichenko et al. simulated the magnetic force and the flow distribution under PMF produced by sine wave current, and the variation in the pulse applying period was investigated [10]. But the variation in the whole period needs to be further investigated. Besides the magnetic force and the flow distribution, the Joule heat produced by the PMF should also be investigated. In this work, the magnetic force distribution, the flow distribution, and Joule heat distribution in the nickel-based superalloy melt under 2.5 Hz PMF produced by the capacitor are researched in the whole pulse period using commercial Ansys finite element software.

2. Mathematical model

2.1. Physical entity and parameter

The PMF casting setup and FEM model used in the simulation are shown in Fig. 1. The PMF casting setup is consisted by the PMF coil, the mold and the melt. We build the FEM model according the PMF casting setup. The current in the coil is a half sine wave, and the pulse current time is 2.8 ms, which is very short compared with the whole period time when the simulated PMF frequency is 2.5 Hz. Therefore, the change in the pulse current can be simplified as linear, which is shown in Fig. 2. The current peak is 8700 A. The parameters used in the magnetic force distribution simulation are shown in Table 1. In the calculation of the flow field distribution, the melt density is 7800 kg/m^3, and the viscosity is 0.0073 Pa s.

2.2. Governing equations

The governing Maxwell equations of electromagnetic field can be expressed in following equations:

$$\nabla \times E = -\partial B/\partial t \quad (1)$$

$$\nabla \cdot B = 0 \quad (2)$$

$$\nabla \cdot D = \rho_0 \quad (3)$$

$$\nabla \times H = J + \partial D/\partial t \quad (4)$$

The constitutive relations for the related electric fields are described in the following equations:

* Corresponding author. Tel.: +86 024 23971728; fax: +86 024 23844528.
E-mail address: ysyang@imr.ac.cn (Y. Yang).

0017-9310/$ - see front matter © 2009 Elsevier Ltd. All rights reserved.
doi:10.1016/j.ijheatmasstransfer.2009.06.042

Nomenclature

B	magnetic flux density vector [Wb m^{-2}]
C_p	specific heat [J kg^{-1} K^{-1}]
D	electric flux density vector [C s^{-2}]
E	electric field intensity vector [V m^{-1}]
f	electromagnetic force [N]
H	magnetic field intensity vector [A m^{-1}]
J	total current density vector [A m^{-2}]
K	thermal conductivity [J kg^{-1} K^{-1}]
p	pressure [Pa]
Q_v	volumetric heat source [J m^{-3} s^{-1}]
t	time [s]
T	temperature [°C]
t_{ij}	stress tensor
u_i	orthogonal velocities ($u_1 = v_x$, $u_2 = v_y$, $u_3 = v_z$) [m s^{-1}]
v	velocity vector [m s^{-1}]
v_x, v_y, v_z	velocity vector components in the x, y and z directions [m s^{-1}]
x, y, z	global Cartesian coordinates

Greek symbols

ε	permittivity [F m^{-1}]
λ	second coefficient of viscosity [kg m^{-1} s^{-1}]
μ	dynamic viscosity [kg m^{-1} s^{-1}]
μ_0	magnetic permeability [H m^{-1}]
ρ_0	electric charge density [C m^{-3}]
σ	conductivity [Ω^{-1} m^{-1}]

Subscripts

I	electric current
MN	minimal value
MX	maximal value
t	time
x, y, z	global Cartesian coordinates

$$J = \sigma(E + v \times B) \tag{5}$$

$$D = \varepsilon E \tag{6}$$

$$B = \mu_0 H \tag{7}$$

The Lorentz force can be acquired according to the following equation:

$$f = \mu_0 J \times H \tag{8}$$

The continuity equation, the momentum equation and the incompressible energy equation are described in Eqs. (9)–(11), respectively.

$$\frac{\partial \rho}{\partial t} + \frac{\partial(\rho v_x)}{\partial x} + \frac{\partial(\rho v_y)}{\partial y} + \frac{\partial(\rho v_z)}{\partial z} = 0 \tag{9}$$

$$\tau_{ij} = -p\delta_{ij} + \mu\left(\frac{\partial u_i}{\partial x_j} + \frac{\partial u_j}{\partial x_i}\right) + \delta_{ij}\lambda\frac{\partial u_i}{\partial x_i} \tag{10}$$

$$\frac{\partial}{\partial t}(\rho C_p T) + \frac{\partial}{\partial x}(\rho V_x C_p T) + \frac{\partial}{\partial y}(\rho V_y C_p T) + \frac{\partial}{\partial z}(\rho V_z C_p T) = \frac{\partial}{\partial x}\left(K\frac{\partial T}{\partial x}\right) + \frac{\partial}{\partial y}\left(K\frac{\partial T}{\partial y}\right) + \frac{\partial}{\partial z}\left(K\frac{\partial T}{\partial z}\right) + Q_v \tag{11}$$

The boundary conditions consistent with the physical entity shown in Fig. 1 are as follows:

Melt top surface $V_y = 0$;
Melt bottom and side surface $V_x = 0$, $V_y = 0$;
Symmetry axis $V_x = 0$.

3. Numerical procedure

Because the PMF is transient and variable, the time dependent simulation is applied. In the simulation, 50 steps are calculated in the periods I, II, IV and V, and the time step is 0.0005 s in the period III. First the vector potential method is applied to calculate the electromagnetic field to get the force distribution and then the result for the magnetic force is coupled with the flow field transient simulation. The plane 53 element is used in the electromagnetic simulation, and 2D flotran 141 element is used in the flow field simulation. The flow field distribution is calculated using the tri-diagonal matrix algorithm [11] (TDMA) iterative solver with laminar model.

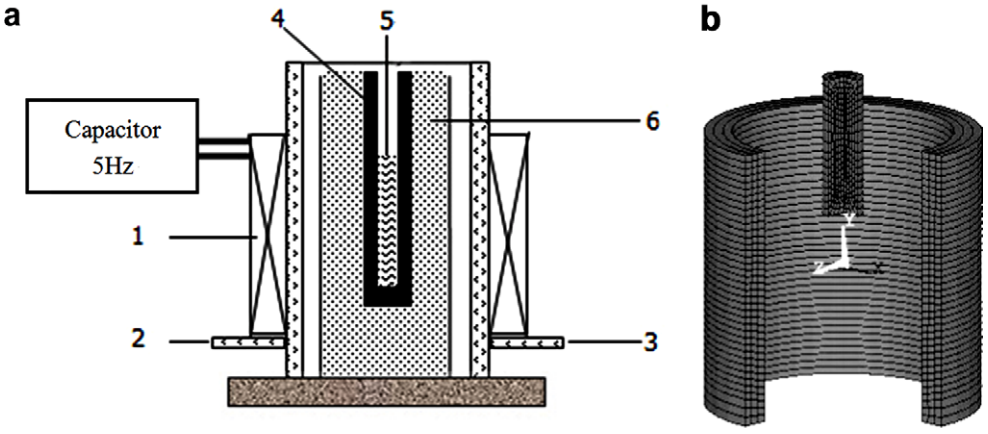

Fig. 1. Sketch of PMF casting setup (a) and FEM model used in the simulation (b). 1. Generator of the pulsed magnetic field, 2. Cooling water inlet, 3. Cooling water outlet, 4. Mold, 5. Melt, 6. Refractory.

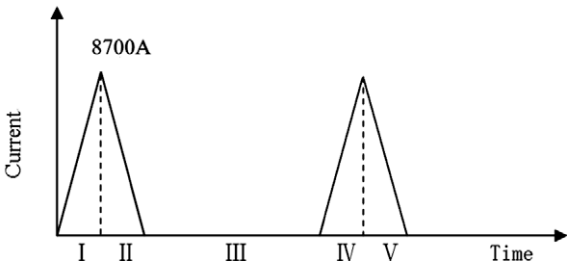

Fig. 2. Variation of pulsed electricity in the coil.

Table 1
Material parameters for simulation.

Material	Resistivity (Ωm)	Permeability
Nickel	6.9×10^{-8}	50
Copper	1.7×10^{-8}	1
Air	–	1

4. Simulation results

4.1. Results for the magnetic force distribution

Periods III, IV, and V are taken as a whole cycle. The magnetic force distribution in the whole period is shown in Figs. 3 and 4.

In the period III, the magnetic pressure force turns to the magnetic pull force, and then the magnetic pressure force appears again. The magnitude of the magnetic force decreases gradually. The largest magnetic force appears near the top of the coil in the early time, and appears near the top and bottom of the melt later. Although magnetic force during period III varies as described above, the magnitude of the magnetic force is far smaller than the force in period IV and V. During period IV, the magnetic pressure force increases to the peak value gradually. In the period V, the value of the magnetic force decreases .In this period, the magnetic pressure force appears inside the melt, while the magnetic pull force appears in the outer part of the melt. During the whole period, mainly the magnetic pressure force appears inside the melt,

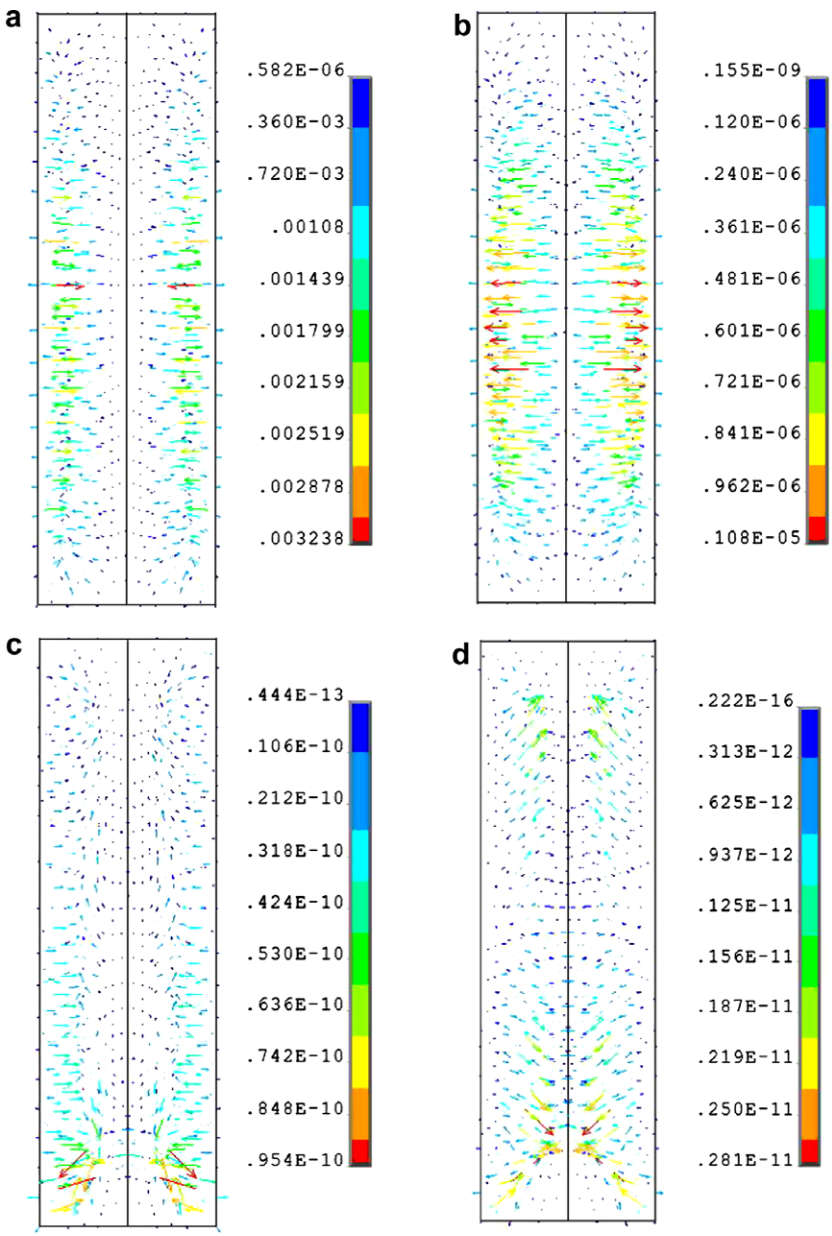

Fig. 3. Magnetic force (N/m^3) distributions in the melt during the pulse diapause period III, (a) step 8 (b) step 40 (c) step 125 (d) step 500.

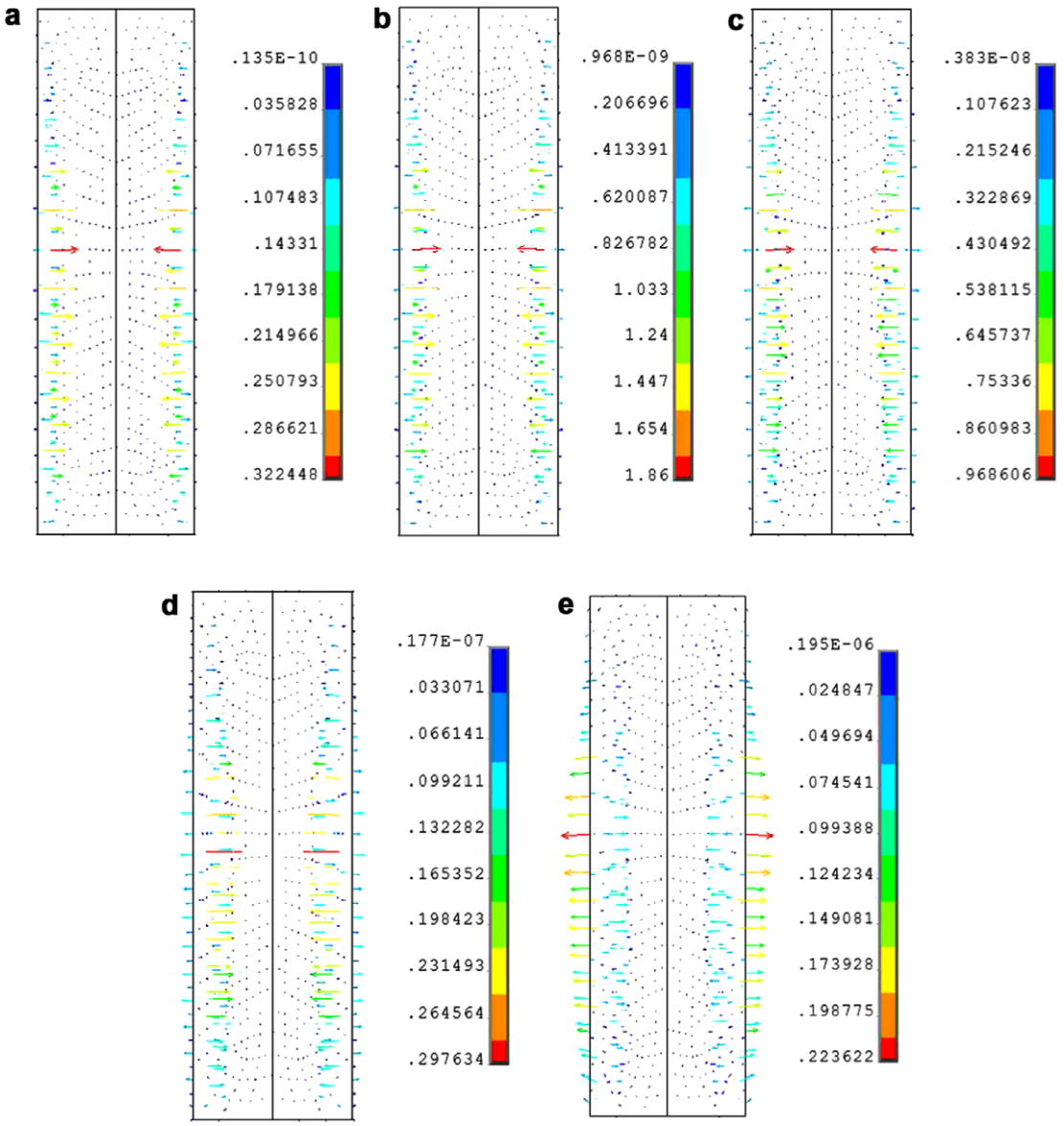

Fig. 4. Magnetic force (N/m^3) distributions in the melt during the pulse applying periods IV and V, (a) period IV – step 15 (b) period IV – step 50 (c) period V – step 5 (d) period V – step 15 (e) period V – step 30.

and there are alternate magnetic pressure force and magnetic pull force in the exterior of the melt.

4.1.1. Results of flow field distribution

Periods III, IV and V are taken as a whole cycle. The flow field distribution in the whole period is shown as Fig. 5. It is obvious that the flow pattern remains identical during the whole period. The convection exists in the whole melt, and the velocity of melt convection is larger at the bottom of the melt than on the top of the melt. The flow velocity increases when the current pulse is applied in period III, and decreases in the diapause of the current pulse in period IV and V.

4.1.2. Results for the Joule heat distribution

Periods III, IV, and V are taken as a whole cycle. The Joule heat distribution in the whole period is shown in Fig. 6. The Joule heat produced by pulsed magnetic field is small during period III. The Joule heat increases with the increase of the PMF in the period IV and decreases with the decrease of the PMF in the period V. It is notable that the Joule heat concentrates near the surface of the melt in period IV and V.

5. Discussion

5.1. Force direction

It can be found according to Fig. 4(e) that the magnetic pressure force and the magnetic pull force exist simultaneously in the melt in the later of period V. This is caused by the skin effect [12]. Because of the skin effect, a vortex will be produced at the surface of the melt, which results in different current direction at the surface and inside the melt. Fig. 7(b) shows the current with different direction in the melt. Therefore, a force with different directions is produced because of different current direction. In period IV and early part of period V, the current direction at the exterior of the melt is consistent with the current direction inside the melt as

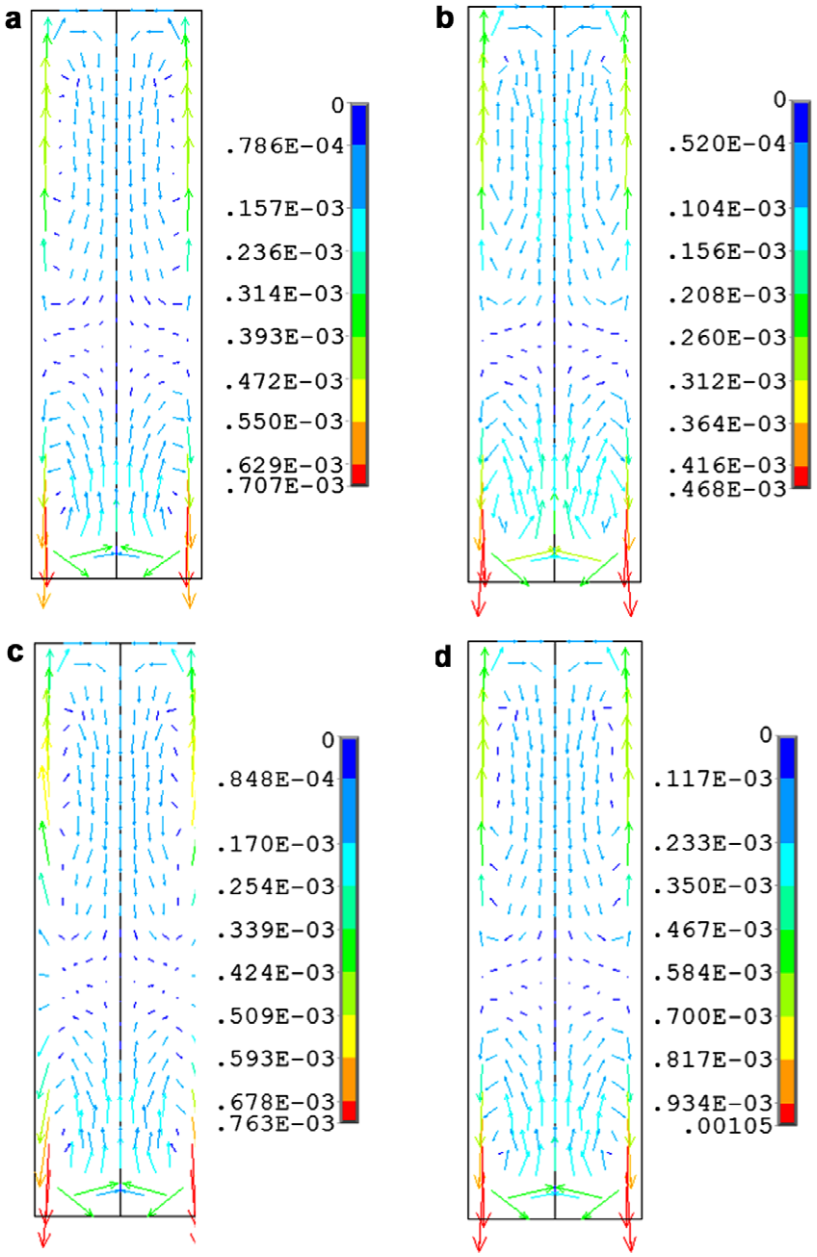

Fig. 5. Flow field (m/s) distributions in the melt, (a) period III – step 15 (b) period III – step 794 (c) period IV – step 50 (d) period V – step 50.

shown in Fig. 7(a). Therefore, only magnetic pressure force exists in the melt.

5.2. The formation of convection and vibration

The magnetic force results show that the main force in the whole period is the magnetic pressure force. The magnetic pressure force can be substituted by a radial direction force and an axial direction force. Fig. 8 shows the *y* direction force. It can be seen that the *y* direction magnetic force concentrates in the exterior of the melt, and the direction of the axial direction magnetic force has reversed direction in different parts of the melt, which produces the convection. In order to verify this conclusion, the magnetic force is simplified. The flow patterns which are simulated keeping the axial direction force and neglecting the axial direction force are shown in Fig. 9. When the axial direction force is neglected, the convection does not form in the whole melt. This means the axial direction magnetic force is the reason for the convection formation.

The surface fluctuation of the melt is observed when PMF is applied, which can be seen in Fig. 10. This fluctuation is caused by the radial direction magnetic force. Because of alternation of the magnetic pressure force and the magnetic pull force in the radial direction in the exterior of the melt, the melt vibrates. The pressure wave in the melt is produced by the diffusion and superposition of vibration, and the pressure wave subsequently produces fluctuation of the melt. Fig. 11(b and c) shows the pressure distribution in the melt when the magnetic pressure force and magnetic pull force are produced. Fig. 11(a) shows the pressure distribution in the melt in the diapause of the pulsed current.

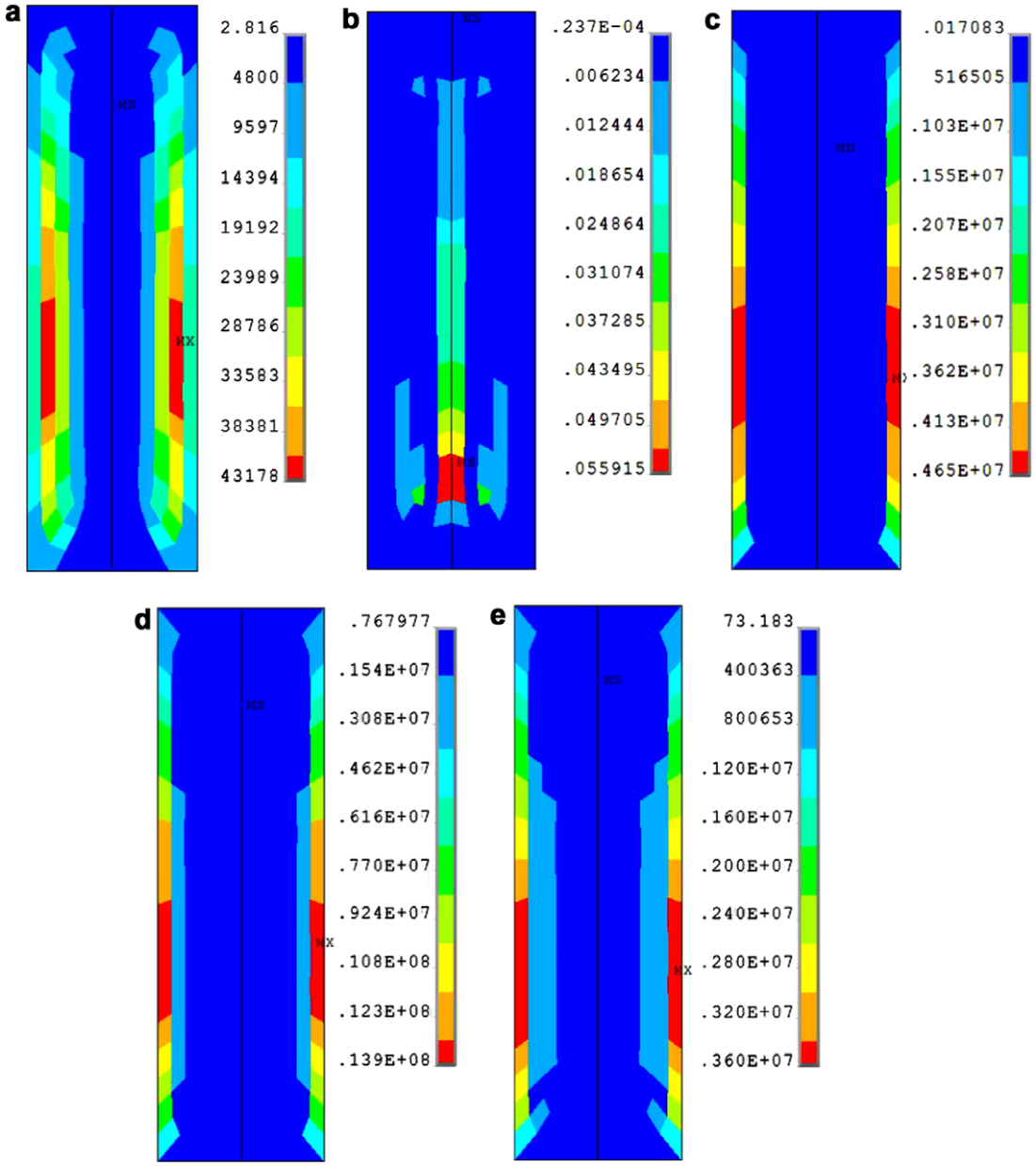

Fig. 6. Joule heat (J/m^3) distributions in the melt, (a) period III – step 7 (b) period III – step 85 (c) period IV – step 15 (d) period IV – step 50 (e) period V – step 30.

6. Conclusion

The magnetic force distribution, the flow field distribution and the Joule heat distribution in the melt under 2.5 Hz PMF were analyzed using transient numerical simulation. The variation of the magnetic force and the flow field distribution with the whole pulsed magnetic period were investigated. The following conclusions are made:

1. The magnetic force is puny in the diapause of the pulsed magnetic field. The magnetic pressure force increases to the peak value with the increase of the PMF. When the PMF decreases, the value of the magnetic force decreases. In this period, the magnetic pressure force appears in the inner of the melt, while magnetic pull force appears in the exterior of the melt. The magnetic pressure force which appears in the exterior of the melt near the top of the coil is the largest in the whole period.
2. The axial direction magnetic force results in the convection in the melt. The radial direction magnetic force produces vibrations in the melt, which diffuses and superposes to produce the pressure wave. The pressure wave causes the fluctuation of the melt.
3. The Joule heat produced by the pulsed magnetic field concentrates near the surface of the melt in period IV and V.
4. Because the vortex current appears in the exterior of the melt, electric currents with different directions appear in different parts of the melt, which results in the magnetic pull force and magnetic pressure force in different parts of the melt.

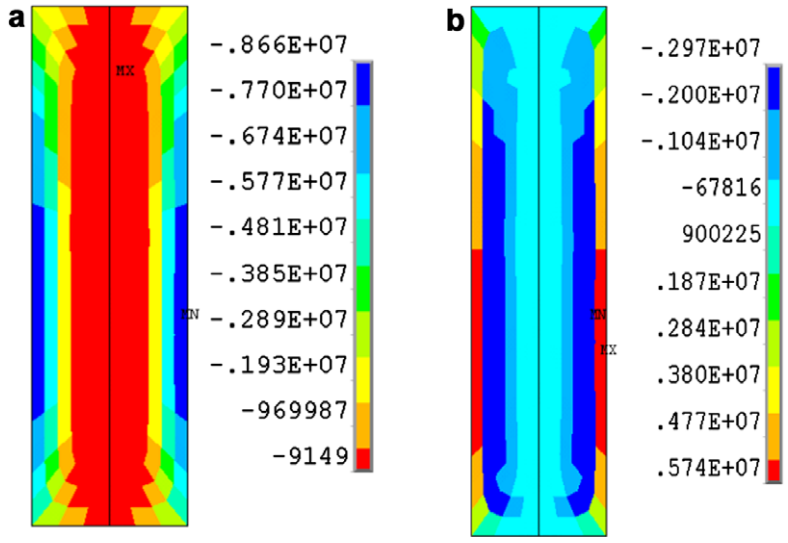

Fig. 7. Current density (A/m^2) distributions in the melt, (a) period V – step 5 (b) period V – step 30.

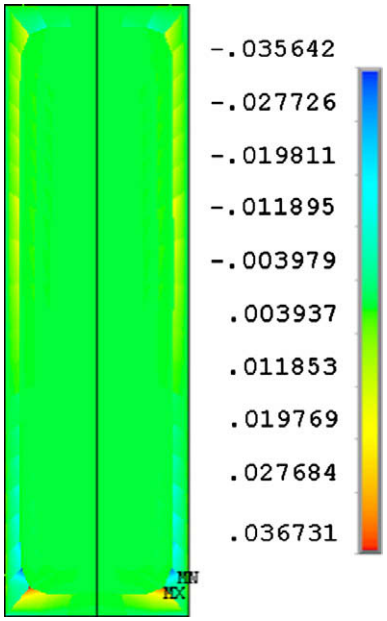

Fig. 8. Distribution of the magnetic force in the axial direction (N/m^3) at step 48 in period I.

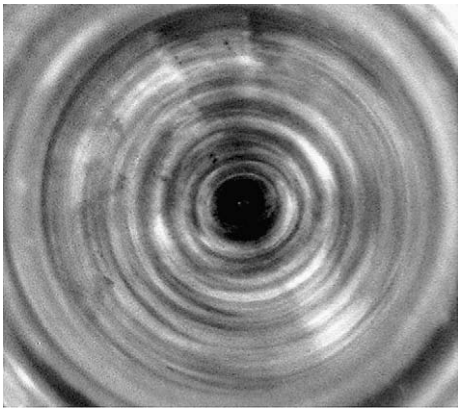

Fig. 10. Fluctuation of mercury surface under PMF.

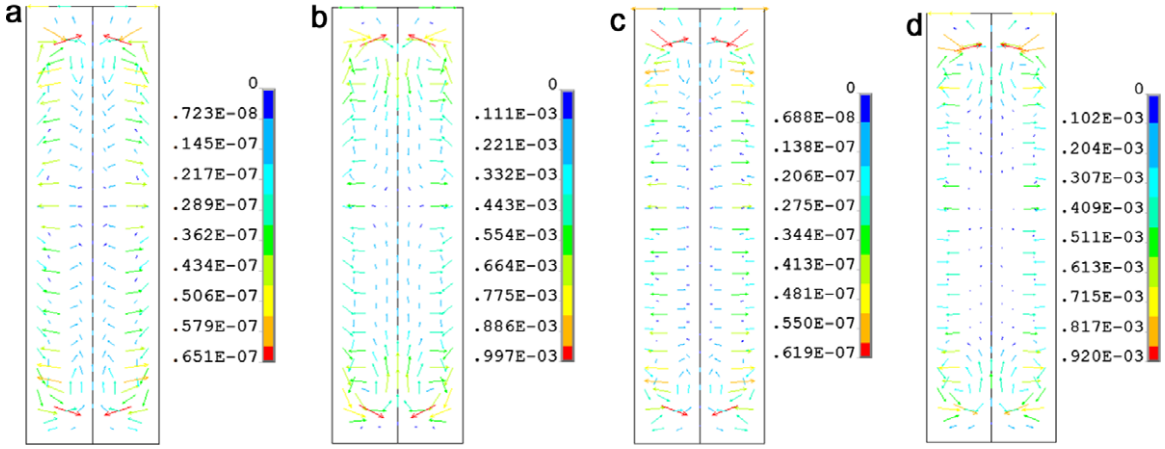

Fig. 9. Flow field (m/s) distributions in the melt keeping the axial direction force and neglecting the axial direction force, (a) step 4, keeping the axial direction force (b) step 39, keeping the axial direction force (c) step 4, neglecting the y direction force (d) step 39, neglecting the axial direction force.

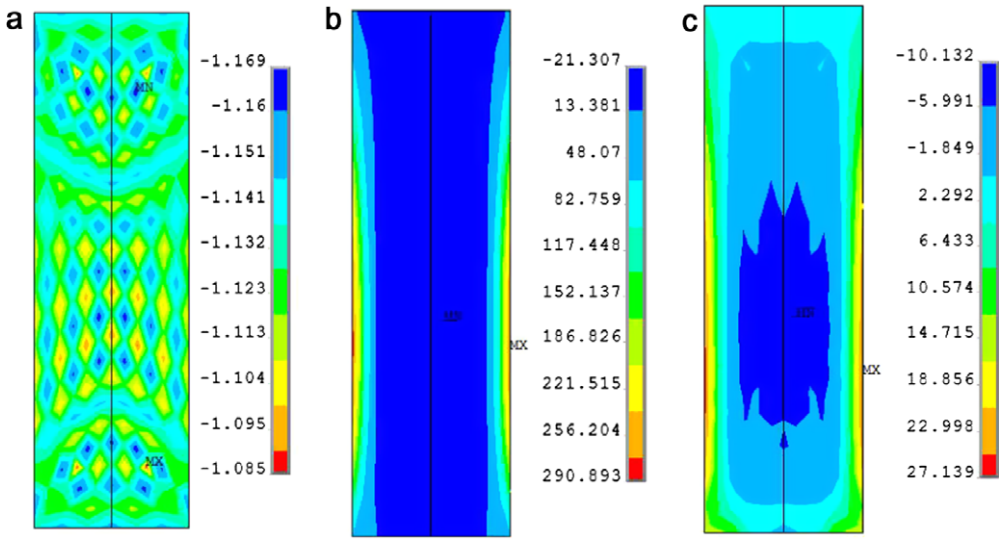

Fig. 11. Distribution of pressure (Pa) in the melt, (a) period III – step 120 (b) period IV – step 50 (c) period V – step 50.

Acknowledgments

The authors gratefully acknowledge the financial support from the National Natural Science Foundation of China (Project No. 50774075).

References

[1] C. Vives, Electromagnetic refining of aluminum alloys by the CREM process: Part 1.Working principle and metallurgical results, Metall. Trans. B 20B (1989) 623–629.
[2] C. Vives, Effect of electromagnetic vibrations on the microstructure of continuously cast aluminum alloys, Mater. Sci. Eng. A 173 (1993) l69–172.
[3] A. Radjai, K. Miwa, Effects of the intensity and frequency of electromagnetic vibrations on the microstructure refinement of hypereutectic A1–Si alloy, Melt. Mat. Mater. Trans. A 31A (2000) 755–762.
[4] Y. Mizutani, T. Tamura, K. Miwa, Microstructural refinement process of pure magnesium by electromagnetic vibrations, Mater. Sci. Eng. A 413–414 (2005) 205–210.
[5] S.J. Guo, Q.C. Le, Z.H. Zhao, Z.J. Wang, J.Z. Cui, Microstructural refinement of DC cast AZ80 Mg billets by low frequency electromagnetic vibration, Mater. Sci. Eng. A 404 (2005) 323–329.
[6] T. Takagi, K. Iwai, S. Asai, Solidified structure of Al alloys by a local imposition of an electromagnetic oscillation force, ISIJ Int. 43 (2003) 842–848.
[7] Y.L. Gao, Q.S. Li, Y.Y. Gong, Q.J. Zhai, Comparative study on structural transformation of low-melting pure Al and high-melting stainless steel under external pulsed magnetic field, Mater. Lett. 61 (2007) 4011–4014.
[8] Q.S. Li, C.J. Song, H.B. Li, Q.J. Zhai, Effect of pulsed magnetic field on microstructure of $1Cr_{18}Ni_9Ti$ austenitic stainless steel, Mat. Sci. Eng. A 466 (2007) 101–105.
[9] B.T. Zi, Q.X. Ba, J.Z. Cui, Study on axial changes of as-cast structures of Al alloy sample treated by the novel SPMF technique, Scr. Mater. 43 (2000) 377–378.
[10] A.F. Kolesnichenko, A.D. Podoltsev, I.N. Kucheryavaya, Action of pulse magnetic field on molten metal, ISIJ Int. 34 (1994) 715–721.
[11] S.V. Patankar, Numerical Heat Transfer and Fluid Flow, Hemisphere, New York, 1980.
[12] K. Hicham, R. Xavier, L. Yvan, Skin effect characterization in a squirrel cage induction machine, IEEE Int. Symp. Ind. Electron. 2 (1997) 532–536.